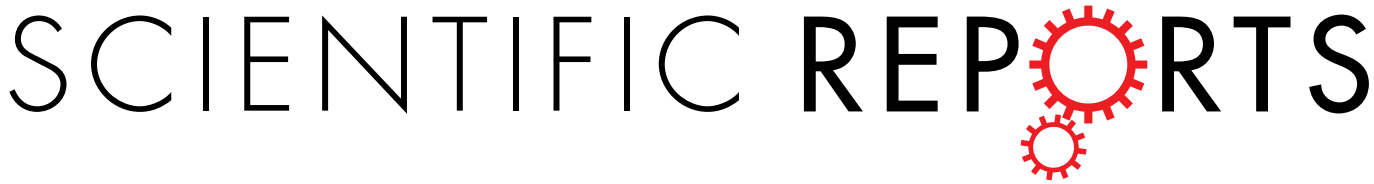

OPEN

Received: 22 May 2017
Accepted: 1 August 2017
Published online: 29 August 2017

Water-assisted and controllable synthesis of core/shell/shell structured carbon-based nanohybrids, and their magnetic and microwave absorption properties

Xiaosi Qi[1,2,3], Erqi Yang[1], Hongbo Cai[1], Ren Xie[1], Zhongchen Bai[1,2], Yang Jiang[1], Shuijie Qin[1,2], Wei Zhong[3] & Youwei Du[3]

By controlling the pyrolysis temperature, core/shell/shell structured Fe/Fe_5C_2/carbon nanotube bundles (Fe/Fe_5C_2/CNTBs), Fe/Fe_3C/helical carbon nanotubes (Fe/Fe_3C/HCNTs) and Fe/Fe_3C/chain-like carbon nanospheres (Fe/Fe_3C/CCNSs) with high encapsulation efficiency could be selectively synthesized in large-scale by water-assisted chemical vapor deposition method. Water vapor was proved to play an important role in the growth process. Because of α-Fe nanoparticles tightly wrapped by two layers, the obtained core/shell/shell structured nanohybrids showed high stabilities and good magnetic properties. The minimum reflection loss values of the as-prepared nanohybrids reached approximately −15.0, −46.3 and −37.1 dB, respectively. The excellent microwave absorption properties of the as-prepared core/shell/shell structured nanohybrids were considered to the quarter-wavelength matching model. Moreover, the possible enhanced microwave absorption mechanism of the as-prepared Fe/Fe_3C/HCNTs and Fe/Fe_3C/CCNSs were discussed in details. Therefore, we proposed a simple, inexpensive and environment-benign strategy for the synthesis of core/shell/shell structured carbon-based nanohybrids, exhibiting a promising prospect as high performance microwave absorbing materials.

With the explosive development of information technology and rapidly expanding use of communication devices, serious electromagnetic (EM) interference pollution has become a great concern, which can cause great disturbances on the medical, industrial, commercial, military equipment and is also potentially harmful to biological systems[1–4]. Therefore, the effective microwave absorbing materials (MAMs) have attracted a great deal of attention in order to attenuate those unwanted EM energies, which is an important issue to be considered for both civil and military purposes[5–8]. Over the past decade, a variety of materials used as microwave absorbers have been extensively studied with an increasing demand for innovative EM interference shielding[9–14]. Recently, considerable attention has been paid to the development of high-efficiency MAMs with light weight, thin thickness, strong absorption characteristics and excellent antioxidant ability[15].

In particular, carbon materials, such as carbon black, graphite flakes, carbon nanotubes (CNTs) and graphene (G), have been explored as promising MAMs, especially in the case of lightweight and harsh environment[16–19]. However, the complex permittivity ($\varepsilon_r = \varepsilon' - j\varepsilon''$) and complex permeability ($\mu_r = \mu' - j\mu''$) of pure carbon materials are out of balance[20,21]. The serious mismatch in the values of ε_r and μ_r will induce that most of the microwave radiation is reflected, rather than absorbed. Based on the impedance matching strategy, one of the effective

[1]College of Physics, Guizhou University, Guiyang, 550025, People's Republic of China. [2]Guizhou Province Key Laboratory for Photoelectrics Technology and Application, Guizhou University, Guiyang City, 550025, People's Republic of China. [3]Nanjing National Laboratory of Microstructures and Jiangsu Provincial Laboratory for NanoTechnology, Nanjing University, Nanjing, 210093, People's Republic of China. Correspondence and requests for materials should be addressed to S.Q. (email: shuijie_qin@sina.com) or W.Z. (email: wzhong@nju.edu.cn)

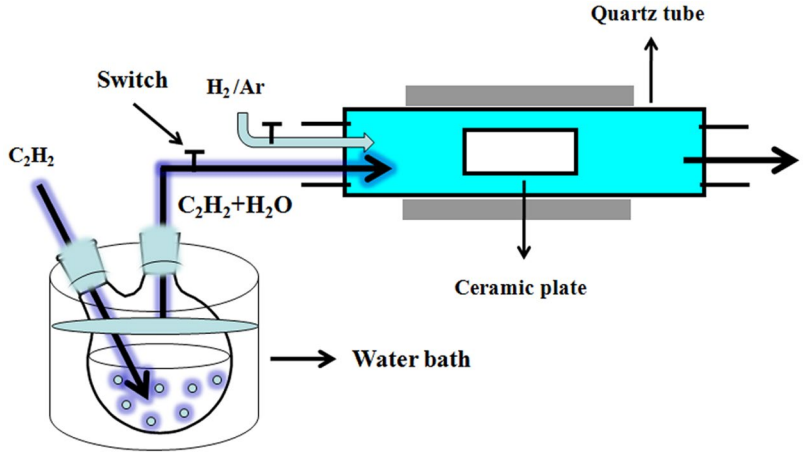

Figure 1. Schematic for the synthesis of core/shell/shell structured nanohybrids.

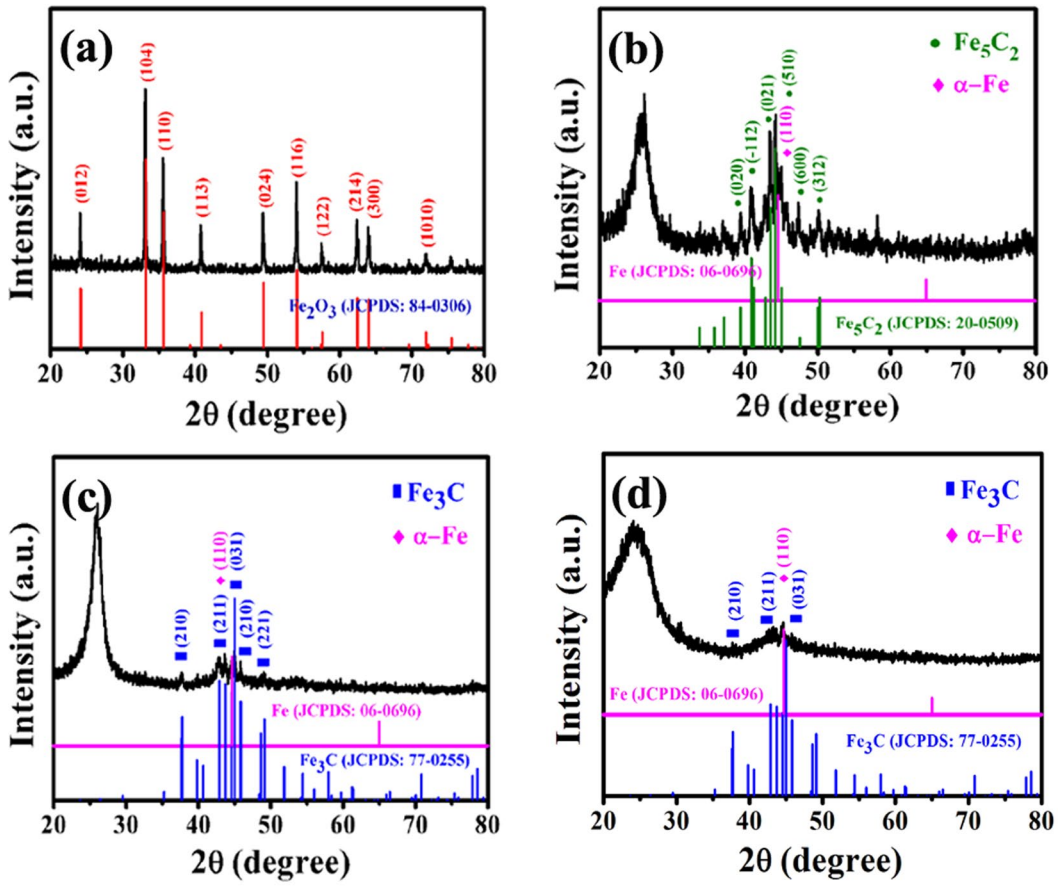

Figure 2. XRD patterns of (**a**) catalyst precursor, (**b**) C-400, (**c**) C-450 and (**d**) C-600.

ways to solve the problem is to incorporate with magnetic nanoparticles. Among these hybrids, core/shell structured magnetic nanoparticles/carbon-based nanohybrids have been proved to exhibit strong EM wave absorption properties because of their interfacial and synergistic effects[22–26]. For example, Wadhawan *et al.* reported that the greater microwave absorption properties of the single-walled CNTs with impurities of magnetic Fe nanoparticles were affected by their cooperative effect[27]. Kim and Che *et al.* synthesized core/shell structured Fe/CNTs, and proved their excellent microwave absorption capabilities, respectively[5,28]. Zhang *et al.* reported that the Ni/C composites exhibited improved microwave absorption properties, which was attributed to the good match between the dielectric loss and magnetic loss[29]. Qu *et al.* found that the enhanced EM wave absorption ability of

Pyrolysis temperature (°C)	400	450	600
Sample	C-400	C-450	C-600
Weight of collected sample in each runs (g)	0.213	1.009	0.860
	0.208	1.013	0.864
	0.212	1.014	0.859

Table 1. Weight of the collected samples at selected temperature in three runs.

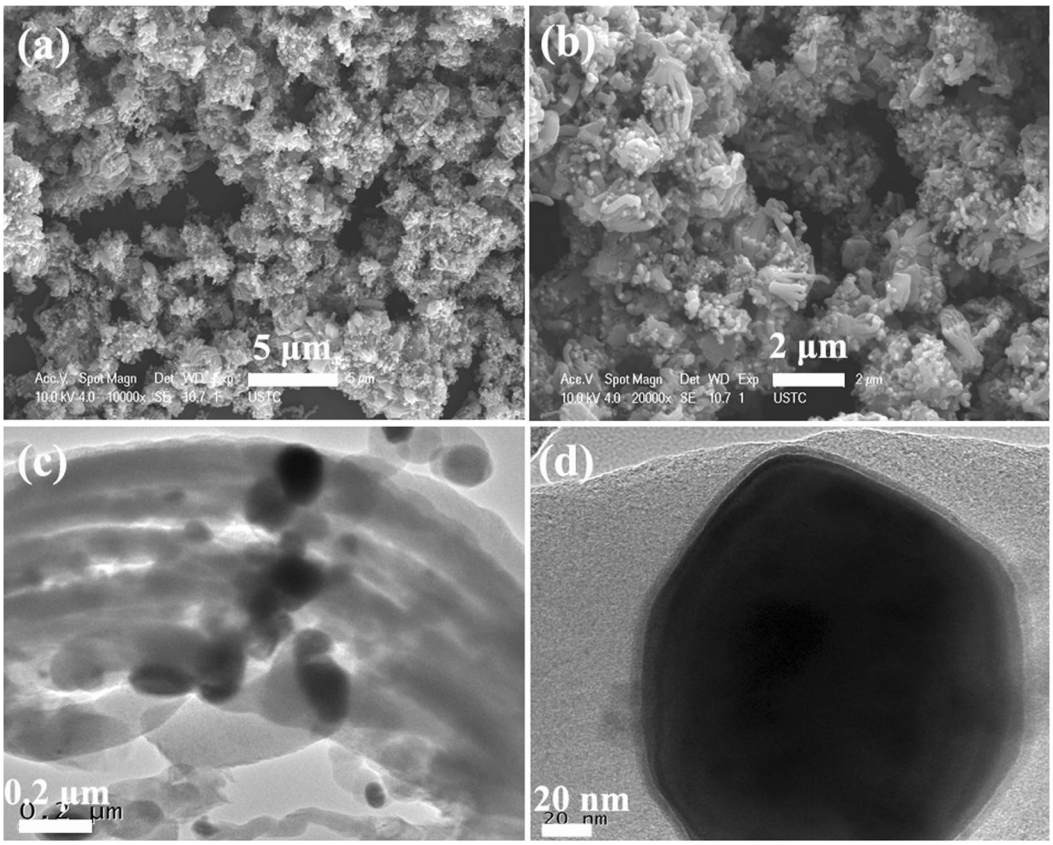

Figure 3. (**a**,**b**) FE-SEM, and (**c**,**d**) TEM images of C-400.

Fe_3O_4-Fe/G composite was ascribed to the well-matched characteristic impedance[30]. So far, various methods and schemes have been proposed to produce core/shell structured magnetic carbon-based nanohybrids, such as chemical vapor deposition (CVD), arc discharge, pulsed laser irradiation of solution, hydrothermal method, and so on[31–35]. Nevertheless, most of these routes available now still suffer from complicated and expensive processes, low capsulation efficiency and uncontrollable synthesis. Therefore, it is desirable to develop a simple, inexpensive and environment-benign strategy for the synthesis of core/shell structured carbon-based nanohybrids with high capsulation efficiency.

Based on the previously reported results[36–40], in this article, we report the selective synthesis of core/shell/shell structured Fe/Fe_5C_2/carbon nanotube bundles (Fe/Fe_5C_2/CNTBs), Fe/Fe_3C/helical carbon nanotubes (Fe/Fe_3C/HCNTs) and Fe/Fe_3C/chain-like carbon nanospheres (Fe/Fe_3C/CCNSs) over Fe nanoparticles by water-assisted CVD method. The results indicate that the introduction of water vapor has a great impact on the yield and morphology of the obtained samples. Due to α-Fe nanoparticles tightly wrapped by two layers and their synergetic effect, the as-prepared Fe/Fe_5C_2/CNTBs, Fe/Fe_3C/HCNTs and Fe/Fe_3C/CCNS show high stabilities, good magnetic properties, and excellent microwave absorption performances.

Results

Figure 1 presents the schematic for the synthesis of core/shell/shell structured nanohybrids. After cooling to room temperature (RT) in Ar, averagely 0.21, 1.01 and 0.86 g of the black sample could be collected in ceramic plate. For easy description, the samples generated at 400, 450 and 600 °C are denoted hereinafter as C-400, C-450 and C-600. Figure 2 shows XRD patterns of the as-synthesized catalyst precursor and samples. As shown in Fig. 2a, the diffraction peaks at 24.1, 33.2, 35.6, 40.9, 49.5, 54.1, 57.5, 62.4, 64.0 and 72.0° can be assigned to (012), (104),

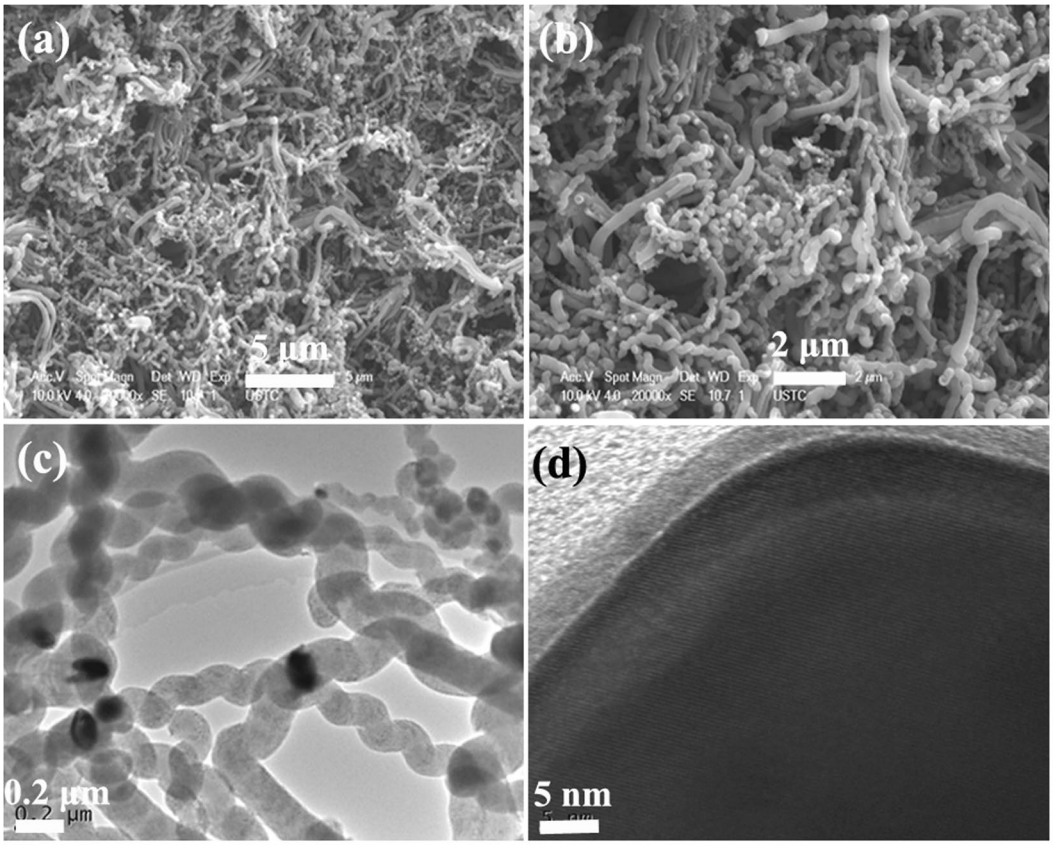

Figure 4. (**a**,**b**) FE-SEM, and (**c**,**d**) TEM images of C-450.

(110), (113), (024), (116), (122), (214), (300), and (1010) crystal planes of Fe_2O_3 (JCPDS No.84-0306). In the absence of signals corresponding to other phases, the result indicates that the catalyst precursor is single-phase α-Fe_2O_3. As indicated by the symbols in Fig. 2b, all the marked diffraction peaks of C-400 correspond to cubic phase of Fe_5C_2 (JCPDS No.20-0509) and cubic phase of α-Fe (JCPDS No.06-0696), respectively. And the diffraction peak at ca. 25.8° corresponding to an interlayer spacing of 0.34 nm, which is attributed to the graphite-like carbon. The XRD patterns of C-450 and C-600 (as shown in Fig. 2c and d) indicate that all the labeled peaks can be indexed to the orthorhombic phase of Fe_3C (JCPDS No.77-0255) and cubic phase of α-Fe (JCPDS No.06-0696), respectively. And the diffraction peak of C-450 and C-600 located at 20–30° is assigned to the encapsulating carbon shell. Based on the obtained XRD results, one can find that C-400 shows higher XRD signals of Fe_5C_2 and α-Fe than those of C-450 and C-600, which may be related to the higher content of Fe_3C and α-Fe in C-400 or/and the thinner encapsulation thickness[41,42]. In the study, as revealed in experimental section, smaller quantity of C-400 could be collected than that of C-450 and C-600 with an equal weight of α-Fe_2O_3 (0.1 g), implying that the highest Fe content of C-400 among the obtained samples. In order to confirm the yields (defined as weight ratio of the collected sample to catalyst) of the obtained samples, each experiment was repeated three times. As shown in Table 1, it can be seen that the designed experiments show an excellent reproducibility and the experimental results are well consistent with the XRD characterizations. Compared to the previously reported Fe/HCNTs[43], much higher yield of sample could be obtained by our proposed route.

Figure 3 presents the microstructure of the as-prepared C-400. The FE-SEM observation (as shown in Fig. 3a and b) reveals that the bright nanodots, which should correspond to the catalyst nanoparticles, are well distributed throughout the obtained carbon nanotube bundles (CNTBs). The TEM investigation (as shown in Fig. 3c) indicates that the catalyst nanoparticles are tightly encapsulated into the tubes of CNTBs. Figure 3d gives a closer TEM image, which displaying evidently that the obtained C-400 exhibits three-layer structure. Based on the obtained results of XRD and microstructure, we can conclude that the as-prepared C-400 is high selectivity of core/shell/shell structured Fe/Fe_5C_2/CNTBs nanohybrid. In order to confirm this result, as shown in Figure S1 (in Supporting Information), the energy dispersive X-ray spectroscopy (EDS) result of the selected area indicates that the elements of C, Fe, O, Pt and Cu can be detected over the obtained C-400. In this study, combined with the sample preparation process before FE-SEM characterization, we think that the C and Fe signal originates from the as-prepared sample, O should be ascribed to the adsorption of H_2O on the obtained sample, Cu signal comes from the copper grid and the spray Pt before the sample characterization induces the appearance of Pt signal. Moreover, The FE-SEM and TEM investigations show that the statistical encapsulation efficiency is ca. 96%. Compared with the schemes reported in the literatures[44–47], the method adopted in this study is simple, inexpensive and high encapsulation efficiency.

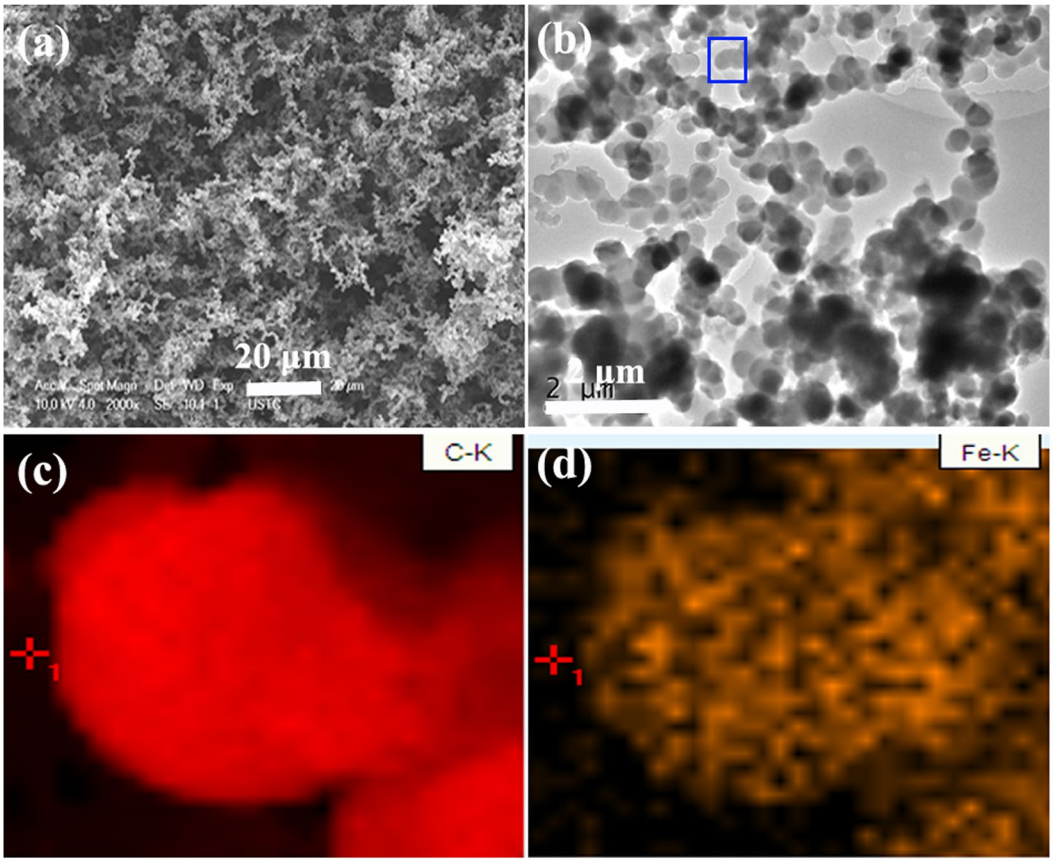

Figure 5. Microstructures of C-600: (**a**) FE-SEM image, (**b**) TEM image (**c**,**d**) EDS elemental mapping of C and Fe from the area as indicated by the green square in (**b**).

The FE-SEM and TEM images of the obtained C-450 are shown in Fig. 4. As displayed in Fig. 4a and b, large scale of helical carbon nanotubes (HCNTs) can be seen evidently and the catalyst nanoparticles (the bright nanodots) are well distributed throughout the obtained sample. Similar to that of C-400, the TEM observation of C-450 (as shown in Fig. 4c and d) indicates that the catalyst nanoparticles are tightly enwrapped by HCNTs and its characteristic of three-layer structure can also be seen clearly. Combined with the results of XRD, we can conclude that the as-prepared C-450 is high selectivity of core/shell/shell structured Fe/Fe_3C/HCNTs nanohybrid. Compared to the previously reported results[44, 48–50], the as-prepared C-450 exhibits an evident structure of core/shell/shell and the obtained yield is high. Moreover, The FE-SEM and TEM investigations show that the morphology of CNTBs can be observed occasionally and the statistical encapsulation efficiency is ca. 95%.

The microstructure of the as-synthesized C-600 is shown in Fig. 5. As shown in Fig. 5a, the FE-SEM observation reveals that the obtained C-600 is spheroidal carbon particles, and the content of such structure is up to 99%. It is apparent that these spheres have the uniform size and their average diameter is ca. 400 nm. According to the classification given by Serp *et al.*[51], the obtained carbon material in the case can be called carbon nanospheres (CNSs). A closer TEM observation (as shown in Fig. 5b) indicates that the obtained carbon nanosphere connects with each other to form chain-like carbon nanospheres (CCNSs) and the catalyst nanoparticles cannot observed obviously. In order to confirm the existence of the catalyst nanoparticles, the selected elemental mapping are conducted. As shown in Fig. 5c and d, the results of element mapping reveal that the as-prepared CNSs are composed of C and Fe. Considering the XRD and TEM results, we think that the as-prepared C-600 should be core/shell/shell structured Fe/Fe_3C/CCNSs nanohybrid. In order to confirm the composition and chemical state of iron, XPS measurement was performed. As shown in Figure S2a, the typical peaks at ca. 284.4 and 285.8 eV can be observed clearly, which can be attributed to the carbon layers in the obtained sample[52]. Similar to that of FeC_x/carbon composites reported elsewhere[52–54], the appearance of C-Fe bonding (283.7 eV) confirms the formation of Fe_3C in the obtained C-600. As shown in Figure S2b, the Fe 2p1/2 and Fe 2p3/2 peaks centered at 709.9 and 723.2 eV can be assigned to Fe^{2+} [52–54], which further indicates that the existence of Fe_3C in the obtained C-600. In addition, compared to the CNSs reported before[55–57], the route proposed by us is a low temperature and feasible scale-up for preparing CNSs. In general, as shown in Table 2, it should be noted that the pyrolysis temperature has a great impact on yield and morphology of the obtained samples and high encapsulation efficiency of core/shell/shell structured nanohybrids can be synthesized by this simple route.

In order to investigate the effect of water vapor, with other experimental conditions kept unchanged, a flow of C_2H_2 was introduced directly (without the supply of H_2O) into the reaction tube and the pyrolysis of acetylene was conducted at 400, 450 and 600 °C for 2 h under atmospheric pressure, respectively. After cooling to

Temperature (°C)	Sample	Yield of product	TEM studies	Efficiency of encapsulation
400	C-400	6.0	Fe/Fe_5C_2/CNTBs	96%
450	C-450	28.8	Fe/Fe_3C/HCNTs	95%
600	C-600	24.6	Fe/Fe_3C/CCNSs	99%

Table 2. Effects of pyrolysis temperature on products.

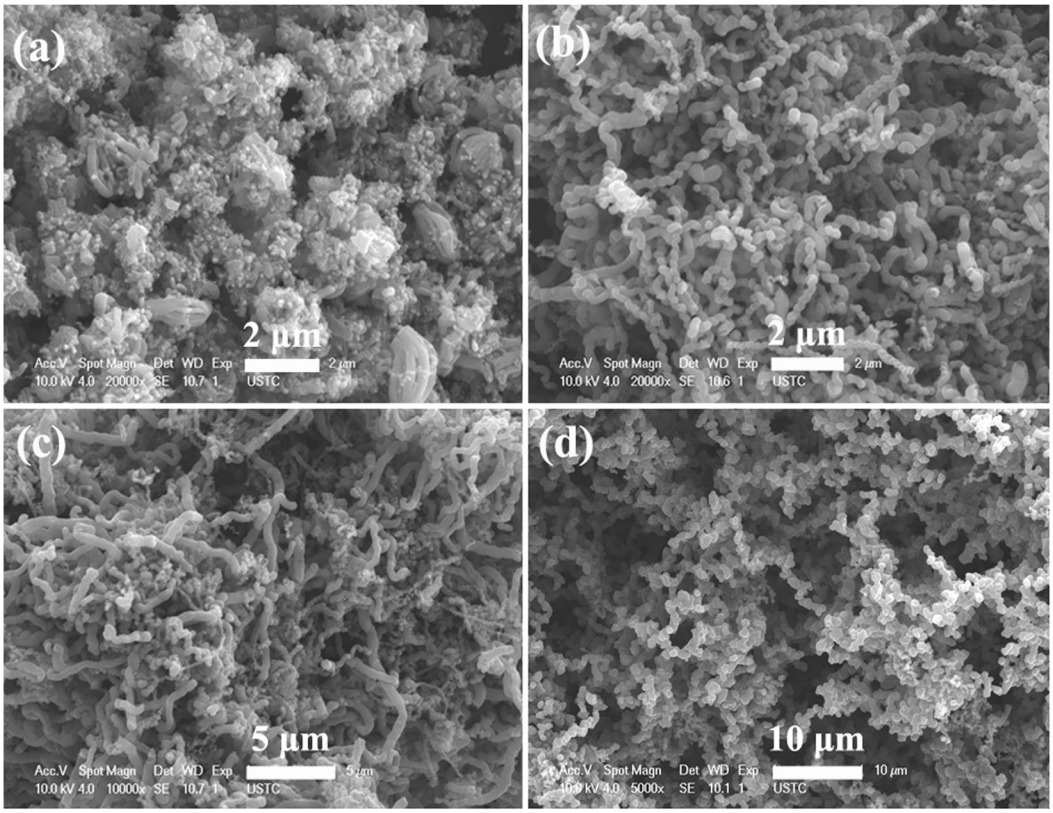

Figure 6. FE-SEM images of the as-prepared samples: (**a**–**c**) at 400, 450 and 600 °C without the addition of water vapor, and (**d**) at 550 °C with the water-assisted catalytic process.

RT, compared to those of C-400, C-450 and C-600, the yield of products obtained at 400 and 450 °C decreases greatly, while the yield of products obtained at 600 °C becomes higher. As shown in Fig. 6a–c, compared to the microstructures of C-400, C-450 and C-600, the TEM and FE-SEM investigations reveal that the introduction of H_2O vapor has a great impact on the morphology of the sample obtained at 600 °C, and this influence on the samples obtained at 400 and 450 °C is little. In order to confirm this effect, additional comparison experiments were designed and conducted: (i) the water-assisted catalytic decomposition of acetylene at 500 and 550 °C for 2 h; (ii) the pyrolysis of acetylene at 500 and 550 °C for 2 h without the supply of H_2O vapor. Compared with the obtained results of experiments (i) and (ii), we can find that the presence of H_2O vapor greatly enhances the yield of samples obtained at 500 and 550 °C, and the morphological change of the sample obtained at 500 °C is unconspicuous. However, similar to that of C-600, the sample synthesized at 550 °C changes from a mixture of CNTs and HCNTs (not shown here) to high selectivity CCNSs (as shown in Fig. 6d) when the water vapor is introduced. As the results reported before[58,59], the introduction of water vapor can greatly improve the growth rate of carbon, which enhances the yield of the as-prepared carbon-based nanohybrids effectively. However, the effect of water vapor on the morphology of the as-prepared carbon materials is rarely reported. Generally, based on the aforementioned results, it can be seen clearly that adding a certain amount of water vapor can greatly improve the yield of the sample obtained at a relatively lower temperature (400–550 °C), and lead to the formation of Fe/Fe_3C/CCNSs in high selectivity at a relatively higher temperature ($>$ 550 °C). According to the obtained results reported by Li and Liu *et al.*[60,61], the effect of H_2O on the synthesis of carbon nanomaterials (CNMs) mainly exhibit two aspects: one is the water vapor can affect the surface energy of facets with higher density of atoms and increase the content of these facets effectively, which is very crucial for the CNM structure. The other is water can act as a weak oxidant for etching excessive amorphous carbon, which favors the growth of CNMs in large scale and high quality. However, excessive addition of water will severely block the formation of CNMs. Based on

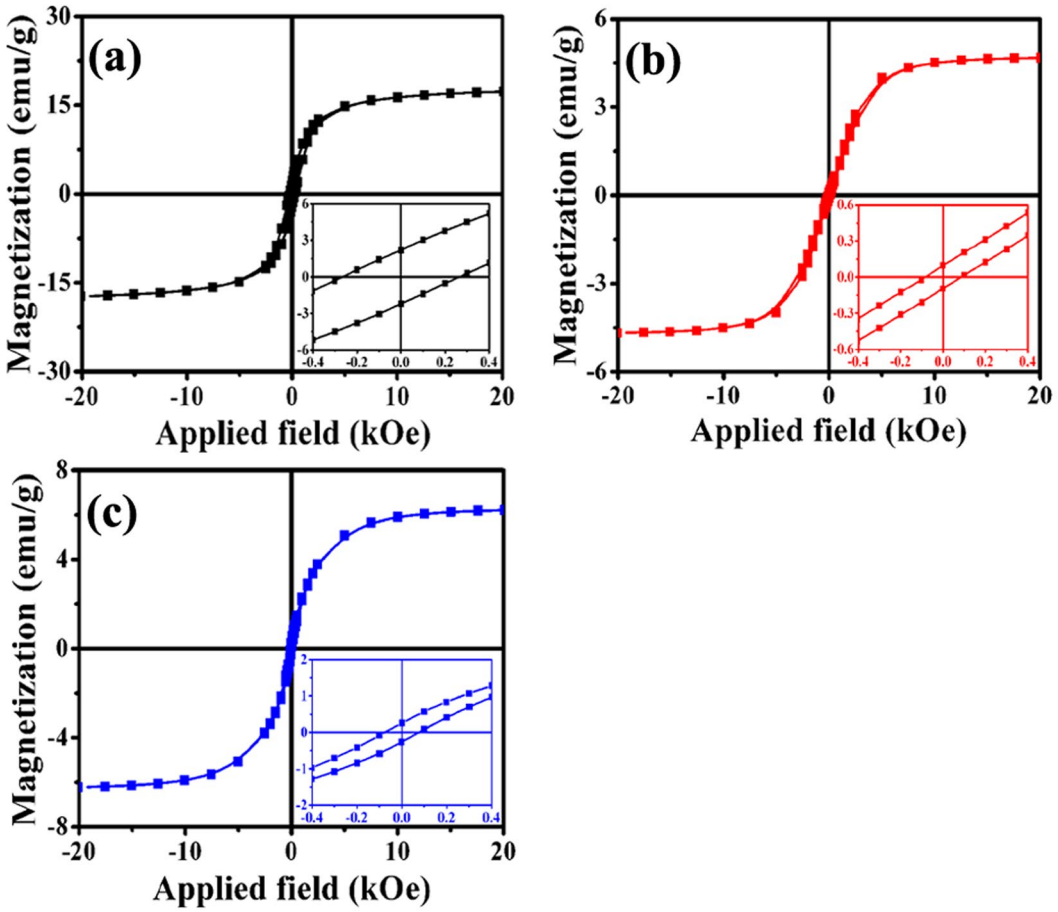

Figure 7. Magnetic hysteresis loop for (**a**) C-400, (**b**) C-450, and (**c**) C-600 at RT (inset is the enlarged part close to the origin).

these reported results, the effect of water vapor on the CNM growth in this study is easily understood. However, because of the complexity, the quantitative study about the effect of water on CNM synthesis is still rarely and requires further investigation.

Figure 7 displays the M-H curves of the obtained samples acquired at 300 K. As shown in Fig. 7a, the saturation magnetization (M_s) and coercivity (H_c) value of C-400 is 17.2 emu/g and 266 Oe, respectively. Compared to those of core/shell nanostructured carbon hybrid reported elsewhere[62,63], the as-synthesized Fe/Fe_5C_2/CNTBs shows an enhanced magnetic property due to the high content of magnetic nanoparticles. The M-H curve of the as-prepared C-450 (as shown in Fig. 7b) indicates that the M_s and H_c value of the sample is 4.7 emu/g and 84 Oe, respectively. While, as shown in Fig. 7c, the M_s value of C-600 is ca. 6.2 emu/g, and its H_c value is 74 Oe. Compared to that of C-400, the small M_s values of C-450 and C-600 can be ascribed to their low content of magnetic nanoparticles as mentioned before. Because of α-Fe tightly wrapped by Fe_5C_2/Fe_3C and the graphitic layer, all the obtained samples showed no changes in XRD patterns and magnetic properties after being kept in air for six months, which implying that the high stabilities of the as-prepared core/shell/shell structured nanohybrids. And the good stabilities and magnetism-tunable properties of the core/shell/shell structured nanohybrids may expand their potential applications in magnetic date storage and human tumor therapy effectively.

Figure 8 gives the complex permittivity and complex permeability of core/shell/shell structured nanohybrids in the 0.5–18.0 GHz frequency range. As shown in Fig. 8a and b, besides some fluctuations, the ε' and ε'' values of the as-prepared nanohybrids are found to decrease with the frequency in the tested region. On the basis of the Debye theory, ε' and ε'' can be described as[64]:

$$\varepsilon' = \varepsilon_\infty + \frac{\varepsilon_s - \varepsilon_\infty}{1 + \omega^2\tau^2} \quad (1)$$

$$\varepsilon'' = \frac{\varepsilon_s - \varepsilon_\infty}{1 + \omega^2\tau^2}\omega\tau + \frac{\sigma_{ac}}{\omega\varepsilon_0} \quad (2)$$

Where ε_s is the static permittivity, ε_∞ is the relative dielectric permittivity at the high frequency limit, ω is angular frequency, τ is polarization relaxation time, σ_{ac} is the alternative conductivity and ε_0 is the dielectric constant in

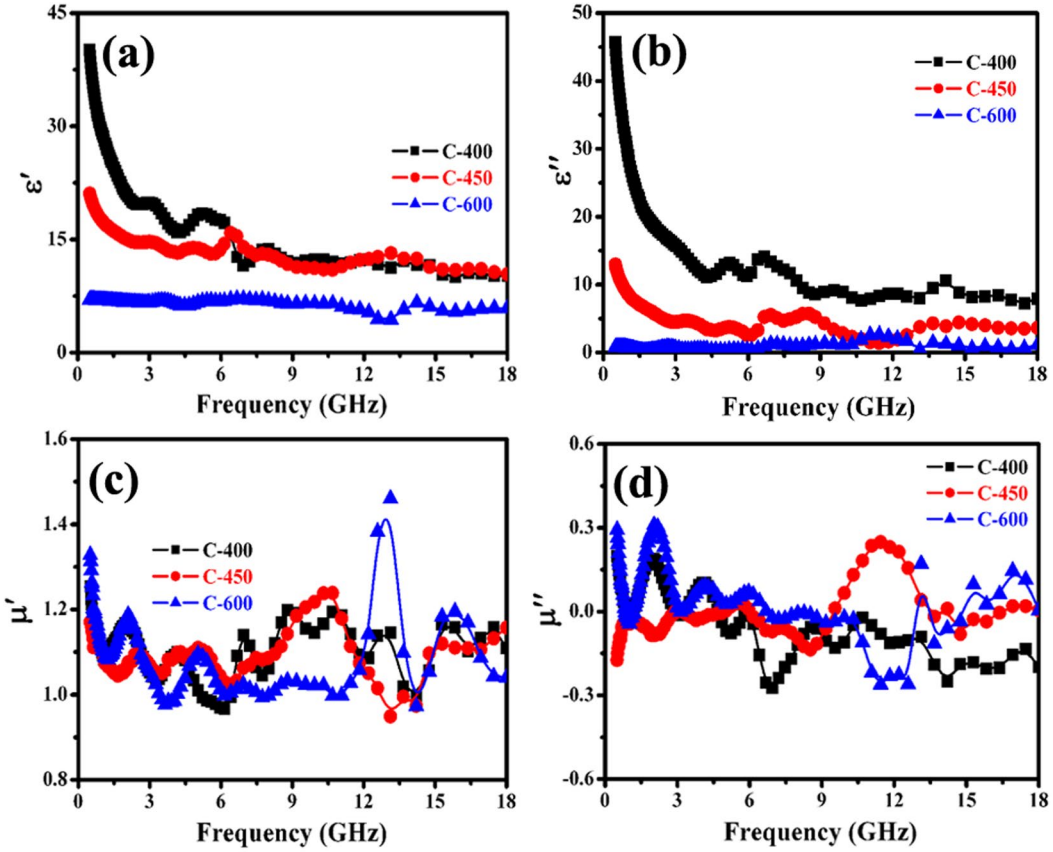

Figure 8. EM parameters of the obtained samples: (**a**) real part, (**b**) imaginary part of permittivity, and (**c**) real part, (**d**) imaginary part of permeability.

vacuum. According to the equations (1) and (2), one can find that the decreases of ε' and ε'' are mainly attributed to the increase of ω. Moreover, it can be seen that the complex permittivity of the obtained hybrids are as follows: C-600 < C-450 < C-400, which implies that the values of ε' and ε'' can be regulated by the pyrolysis temperature and this discrepancy can be explained that the different electric polarization and conductivity properties of the as-synthesized carbon materials[65,66]. Figure 8c and d present the complex permeability of as-prepared nanohybrids as a function of frequency. Like the previously reported core/shell structured nanohybrids[67–69], we can see that the values of μ' and μ'' have some marked fluctuations and their discrepancy is unobvious in the whole frequency range, which may be related to the uneven size of catalyst nanoparticles and the little difference in magnetization as mentioned above. Moreover, we can notice that the μ'' values are negative in the specific frequency range, which suggests that the EM wave absorption mechanism is attributed to both magnetic loss and dielectric loss[69,70].

According to the transmission line theory, the values of reflection loss (RL) and attenuation constant (α) are calculated by the following equations[71,72]:

$$Z_{in} = \sqrt{\frac{\mu_r}{\varepsilon_r}} \tanh\left(j\frac{2\pi f d\sqrt{\mu_r\varepsilon_r}}{c}\right) \tag{3}$$

$$RL = 20\log\left|\frac{Z_{in}-1}{Z_{in}+1}\right| \tag{4}$$

$$\alpha = \frac{\sqrt{2}\pi f}{c}\sqrt{(\mu''\varepsilon'' - \mu'\varepsilon') + \sqrt{(\mu''\varepsilon'' - \mu'\varepsilon')^2 + (\varepsilon'\mu'' + \varepsilon''\mu')^2}} \tag{5}$$

where f is the frequency of EM wave, d is the thickness of absorber, c is the velocity of light and Z_{in} is the input impedance of absorber. Based on the equations (3) and (4), the RL of the as-prepard nanohybrids could be obtained and shown in Fig. 9. As shown in Fig. 9a, one can observe that the minimal RL value of C-400 is ca. −15.0 dB at 17.5 GHz with a matching thickness of 1.23 mm. And the RL values below −10 dB, which indicates 90% of EM wave energy is attenuated by the absorber, can be obtained in the frequency range of 7.7–18.0 GHz.

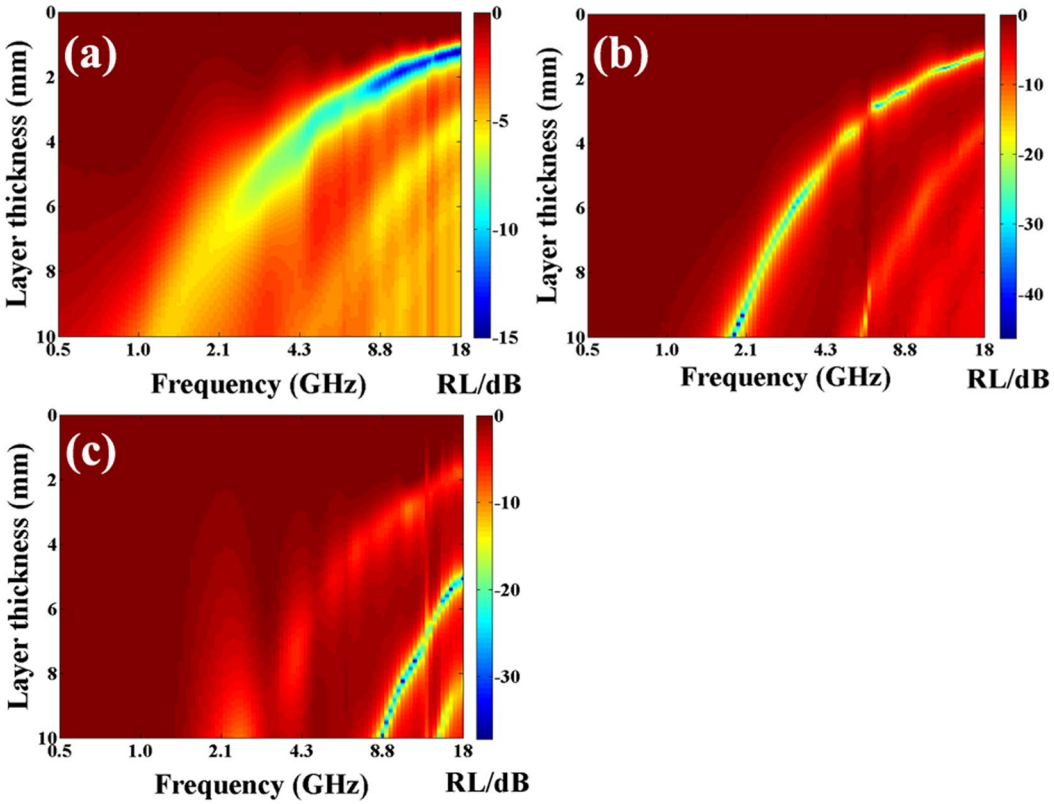

Figure 9. Two-dimensional representation RL values for (**a**) C-400, (**b**) C-450, and (**c**) C-600, respectively.

Figure 9b shows that the optimal RL value of C-450 is ca. −46.3 dB at 1.9 GHz, and the absorption bandwidth with RL values less than −20 dB (99% of EM wave energy absorption) can be obtained in the frequency range of 1.8–3.9 and 6.7–18.0 GHz. As shown in Fig. 9c, it can be seen that the minimal RL value of C-600 is ca. −37.1 dB at 16.4 GHz, and the absorption bandwidth with RL values less than −20 dB is 9.2 GHz (from 8.8 to 18.0 GHz). Generally, as shown in Table 3, the microwave absorption performance of the obtained hybrids is as follows: C-450 > C-600 > C-400. In addition, compared to those of the representative magnetic carbon-based nanohybrids[73–80], the as-prepared core/shell/shell structured nanohybrids here exhibit enhanced microwave absorption properties. In other words, these obtained nanohybrids can be used as the lightweight and excellent MAMs alternative to these previously reported EM wave absorption materials.

Discussion

In order to analyze the possible enhanced microwave mechanism of the as-prepared C-450 and C-600, the dielectric and magnetic loss properties, attenuation constant and impedance matching of the obtained nanohybrids were investigated in details. As shown in Fig. 10a and b, the as-prepared nanohybrids exhibit very strong dielectric loss and relatively weak magnetic loss over the whole tested frequency range, implying that the excellent EM wave attenuation is mainly due to dielectric loss. Overall, the dielectric loss performance (as shown in Fig. 10a) of the hybrids presents the following tendency: C-400 > C-450 > C-600. According to equation (5), the α values of the as-prepared nanohybrids are shown in Fig. 10c. It can be seen that all the as-prepared C-400 exhibits the highest α value while the α value of C-600 is the lowest. In addition, compared to the previously reported Fe/MWCNTs, Co/MWCNTs, Ni/MWCNTs and MnO_2/Fe-G[73,79], the α values of the obtained core/shell/shell structured nanohybrids are much higher, which is conducive to improve EM wave absorption capability[72]. Based on the measured complex permittivity and permeability, the impedance matching ratios of nanohybrids are obtained and the results are displayed in Fig. 10d. Due to the contribution of magnetic nanoparticles, the impedance matching ratio of the nanohybrids presents the following tendency: C-600 > C-450 > C-400. Based on the aforementioned results, we can find that the enhanced microwave absorption capabilities of Fe/Fe_3C/HCNTs and Fe/Fe_3C/CCNSs are mainly attributed to the better impedance matching properties. Combined the previously reported papers with our obtained results[81,82], the improved impedance matching ratio of C-600 and C-450 should be related to their special structure and synergetic effect.

As shown in Fig. 9 and Table 3, one can find that the as-prepared core/shell/shell structured nanohybrids exhibit excellent microwave absorption properties. Recently, two models such as zero reflection and geometrical effect have been proposed to explain the excellent EM wave absorption properties of MAMs[9,72]. For zero reflection, the relationship $\mu_r = \varepsilon_r$ should be satisfied in terms of EM wave theory[9]. However, as shown in Fig. 8, the permittivity of the as-prepared nanohybrids is much higher than their permeability, which indicating that the obtained results cannot be interpreted by this model. As for the geometrical effect, it takes place when the incident

Sample	Optimal RL value (dB)	Frequency range (GHz) (RL < −10 dB)	Frequency range (GHz) (RL < −20 dB)	Reference
Fe/MWCNTs[a]	−39	1.0–6.0	2.04–3.47	73
Fe_3O_4/C	−27.9	5.0–18.0	4.5–6.5	74
Fe_3O_4/TiO_2	−20.6	2.5–18.0	5.0–9.0	75
Fe_3O_4/CNTs	−41.6	3.0–11.4	4.4–7.5	76
Fe/HCNTs	−43.4	2.0–18.0	6.67–9.17, 15.83–18.0	77
Fe/G	−45	4.2–18.0	5.0–17.8	78
Fe/MnO_2-G	−17.5	5.0–18.0	—	79
ZnO/Fe/Fe_3O_4/G	−38.4	5.0–18.0	5.9–15.2	80
Fe/Fe_5C_2/CNTBs (C-400)	−15.0	7.7–18.0	—	This work
Fe/Fe_3C/HCNTs (C-450)	−46.3	1.7–18.0	1.8–3.96.7–18.0	This work
Fe/Fe_3C/CCNSs (C-600)	−37.1	8.3–18.0	8.8–18.0	This work

Table 3. Summary of the representative core/shell structured carbon-based MAMs reported in recent papers. Fe/multiwalled CNTs[a].

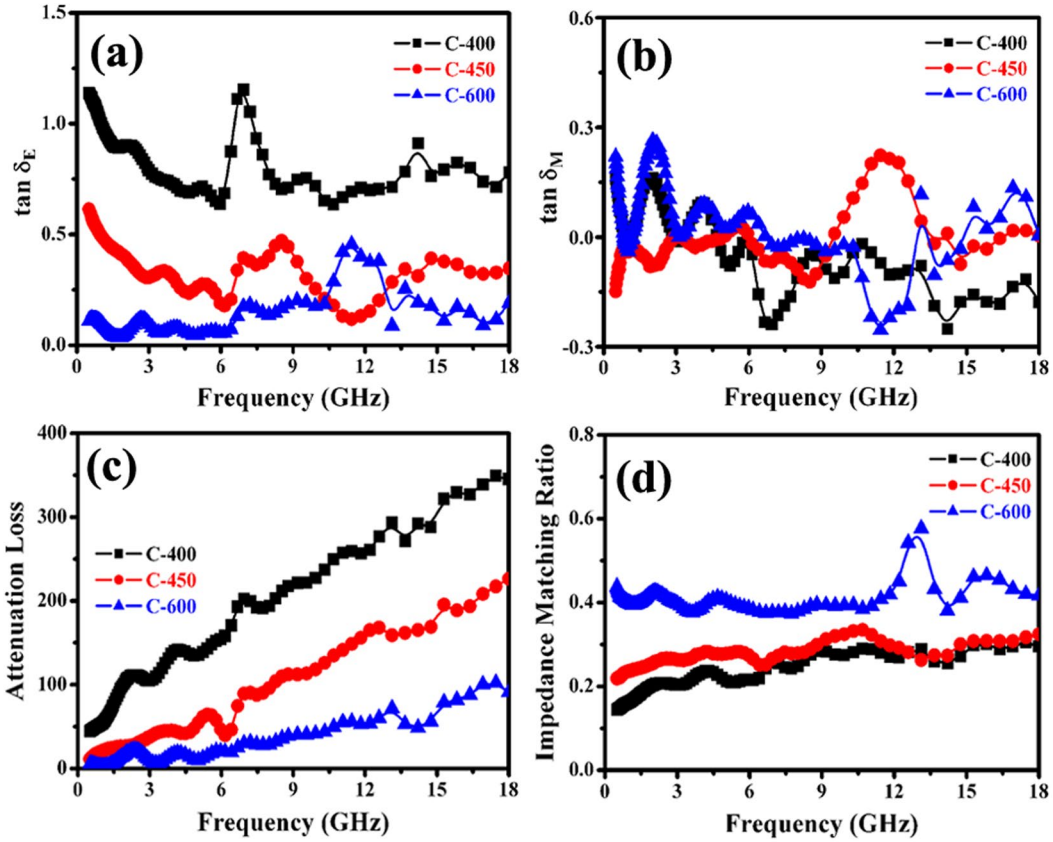

Figure 10. (**a**,**b**) Loss tangent, (**c**) attenuation loss, and (**d**) impedance matching of Fe/carbon-based nanohybrids.

and reflected waves in the absorbers are out of phase by 180°. This effect is strongly dependent on the quarter-wavelength equation[83]:

$$d_m = nc/4f_m\sqrt{|\mu_r||\varepsilon_r|} \qquad (n = 1, 3, 5\cdots) \tag{6}$$

Here, $|\mu_r|$ and $|\varepsilon_r|$ are the modulus of the measured μ_r and ε_r at f_m, respectively. According to the model, if the matching thickness of the absorber satisfies the equation (6), the two emerging reflected EM waves from the air-absorber interface and absorber-metal interface are out of phase by 180°. And the absorber can exhibit excellent EM wave absorption property due to the extinction of EM wave on the air-absorber interface. According to equation (6), the d_m can be simulated, which denoted as d_m^{sim}, and the results are shown in Fig. 11. It is clearly found that the obtained d_m^{sim} are in good agreement with the values of d_m^{exp} (directly achieved from the RL curves

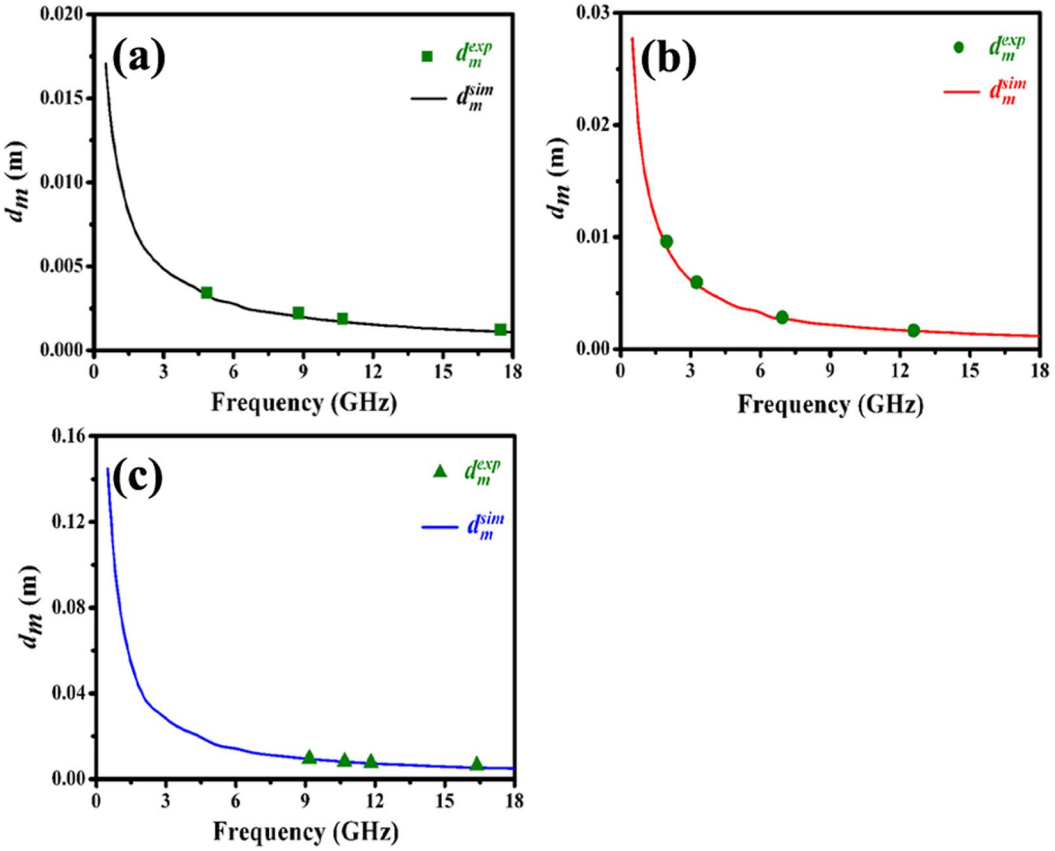

Figure 11. Comparison of the simulated matching thickness (d_m^{sim}) with the d_m^{exp} obtained from RL values shown in Fig. 9.

in Fig. 9). Therefore, same to Fe_3O_4-Fe/G, Fe_3O_4/C and G/PANI/porous TiO_2 reported recently[30,84,85], the excellent microwave absorption properties of as-prepared nanohybrids can be explained by the quarter-wavelength matching model.

In summary, a simple and effective water-assisted approach is developed for the synthesis of core/shell/shell structured carbon-based nanohybrids with high encapsulation efficiency. By controlling the pyrolysis temperature, Fe/Fe_5C_2/CNTBs, Fe/Fe_3C/HCNTs and Fe/Fe_3C/CCNSs can be selectively synthesized in large-scale. Water vapor is considered to play an important role in the growth process. Because of α-Fe nanoparticles tightly wrapped in two layers, the obtained core/shell/shell structured nanohybrids show high stabilities and good magnetic properties. Moreover, the obtained results indicate that the as-prepared core/shell/shell structured nanohybrids exhibit excellent microwave absorption properties due to the quarter-wavelength matching model. Due to their special structure and synergetic effect, the as-prepared Fe/Fe_3C/HCNTs and Fe/Fe_3C/CCNSs exhibit better impedance matching and enhanced microwave absorption performances as compared to Fe/Fe_5C_2/CNTBs, which may be promising candidate for light-weight and high performance MAMs.

Method

Synthesis of catalyst precursor. Similar to the method reported previously[48], 0.01 mol $FeCl_2{\cdot}4H_2O$ and 0.015 mol citric acid monohydrate were well mixed with 100 mL of absolute ethanol and stirred at 60 °C for 6 h. The mixture was heated at 80 °C until the formation of xerogel, and the obtained xerogel was then heated in air at 450 °C for 4 h for the generation of ferric oxide.

Synthesis of core/shell/shell structured nanohybrids. As shown in Fig. 1, 50 mg of the ferric oxide powder was dispersed on a ceramic plate and placed inside a quartz reaction tube. At the beginning of the reaction, Ar gas was flowed into the quartz CVD reactor to purge the reactor before the furnace was heated up to the temperature of 450 °C. After the furnace temperature was stable, Ar was turned-off and H_2 was allowed to the reaction chamber. After the reduction of ferric oxide in H_2 at 450 °C for 1 h, the gas supply was shifted from H_2 to acetylene and a flow of C_2H_2 through a water bubbler (heated at 40 °C in water bath) was introduced into the reaction tube and the pyrolysis of acetylene was conducted at 400, 450 and 600 °C for 2 h under atmospheric pressure, respectively. After cooling to room temperature (RT) in Ar, averagely 0.21, 1.01 and 0.86 g of the black sample could be collected in each run. For easy description, the samples generated at 400, 450 and 600 °C are denoted hereinafter as C-400, C-450 and C-600, respectively.

Characterization. The samples were examined on an X-ray powder diffractometer (XRD) at RT for phase identification using CuK_{α} radiation (model D/Max-RA, Rigaku). The morphology investigations were examined using a field emission scanning electron microscope (FE-SEM) (model FEI Sirion 200, operated at accelerating voltages of 5 kV) and transmission electron microscope (TEM) (model Tecnai-G20, operated at an accelerating voltage of 20 kV). The X-ray photoelectron spectroscopy (XPS) data were taken on a VG Multilab2000 spectrometer. The magnetic properties of samples were measured at 300 K using a Quantum Design MPMS SQUID magnetometer (Quantum Design MPMS-XL) equipped with a superconducting magnet capable of producing fields of up to 50 kOe. For microwave measurement, 30 wt% of the as-prepared samples were mixed with paraffin and pressed into coaxial clapper in a dimension of outer diameter of 7.0 mm, inner diameter of 3.0 mm, respectively. The complex permittivity ($\varepsilon_r = \varepsilon_r' - j\varepsilon_r''$) and complex permeability ($\mu_r = \mu_r' - j\mu_r''$) of the composites were measured in frequency range of 0.5–18 GHz over an Agilent E8363B vector network analyzer.

References

1. Liu, X. G., Jiang, J. J., Geng, D. Y. & Li, B. Q. Dual nonlinear dielectric resonance and strong natural resonance in Ni/ZnO nanocapsules. *Appl. Phys. Lett.* **94**, 053119 (2009).
2. Wang, Y. M., Li, T. X., Zhao, L. F., Hu, Z. W. & Gu, Y. J. Research progress on nanostructured radar absorbing materials. *Energy Power Eng.* **3**, 580–584 (2011).
3. Qin, F. & Peng, H. X. Ferromagnetic microwires enabled multifunctional composite materials. *Prog. Mater. Sci.* **58**, 183–259 (2013).
4. Girgert, R., Grundker, C., Emons, G. & Hanf, V. Electromagnetic fields alter the expression of estrogen receptor cofactors in breast cancer cells. *Bioelectromagnetics* **29**, 169–176 (2008).
5. Che, R. C., Peng, L. M., Duan, X. F., Chen, Q. & Liang, X. L. Microwave absorption enhancement and complex permittivity and permeability of Fe encapsulated within carbon nanotubes. *Adv. Mater.* **16**, 401–405 (2004).
6. Thomassin, J. M. *et al*. Multiwalled carbon nanotube/poly(ε-caprolactone) nanocomposites with exceptional electromagnetic interference shielding properties. *J Phys. Chem. C* **111**, 11186–11192 (2007).
7. An, Z. G., Pan, S. L. & Jiang, J. J. Facile synthesis and characterization of glass/cobalt core/shell composite spheres with tunable shell morphologies. *Appl. Surf. Sci.* **256**, 1976–1982 (2010).
8. Xu, P. *et al*. Synthesis and characterization of novel coralloid polyaniline/$BaFe_{12}O_{19}$ nanocomposites. *J. Phys. Chem. C* **111**, 12603–12608 (2007).
9. Liu, J. W. *et al*. Microwave absorption enhancement of multifunctional composite microspheres with spinel Fe_3O_4 cores and anatase TiO_2 shells. *Small* **8**, 1214–1221 (2012).
10. Cui, C. K. *et al*. Synthesis of electromagnetic functionalized Fe_3O_4 microspheres/polyaniline composites by two-step oxidative polymerization. *J. Phys. Chem. B* **116**, 9523–9531 (2012).
11. Saini, P. *et al*. High permittivity polyaniline-barium titanate nanocomposites with excellent electromagnetic interference shielding response. *Nanoscale* **5**, 4330–4336 (2013).
12. Ren, Y. L. *et al*. Three-dimensional SiO_2@Fe_3O_4 core/shell nanorod array/graphene architecture: synthesis and electromagnetic absorption properties. *Nanoscale* **5**, 12296–12303 (2013).
13. Liu, J. W. *et al*. Double-shelled yolk–shell microspheres with Fe_3O_4 cores and SnO_2 double shells as high-performance microwave absorbers. *J. Phys. Chem. C* **117**, 489–495 (2013).
14. Saini, P., Choudhary, V., Vijayan, N. & Kotnala, R. K. Improved electromagnetic interference shielding response of poly(aniline)-coated fabrics containing dielectric and magnetic nanoparticles. *J. Phys. Chem. C* **116**, 13403–13412 (2012).
15. Singh, V. *et al*. Microwave absorbing properties of a thermally reduced graphene oxide/nitrile butadiene rubber composite original. *Carbon* **50**, 2202–2208 (2012).
16. Liu, X. G. *et al*. (Fe, Ni)/C nanocapsules for electromagnetic-wave-absorber in the whole Ku-band. *Carbon* **47**, 470–474 (2009).
17. Tang, N. J. *et al*. Synthesis, microwave electromagnetic, and microwave absorption properties of twin carbon nanocoils. *J. Phys. Chem. C* **112**, 19316–19323 (2008).
18. Huang, L. N., Liu, X. F., Chuai, D., Chen, Y. X. & Yu, R. H. Flaky FeSiAl alloy-carbon nanotube composite with tunable electromagnetic properties for microwave absorption. *Sci. Rep.* **6**, 35377 (2016).
19. Zhao, S. C. *et al*. Alternate nonmagnetic and magnetic multilayer nanofilms deposited on carbon nanocoils by atomic layer deposition to tune microwave absorption property. *Carbon* **98**, 196–203 (2016).
20. Wang, C. *et al*. The electromagnetic property of chemically reduced graphene oxide and its application as microwave absorbing material. *Appl. Phys. Lett.* **98**, 072906 (2011).
21. Qi, X. S. *et al*. Metal-free carbon nanotubes: synthesis, and enhanced intrinsic microwave absorption properties. *Sci. Rep.* **6**, 28310 (2016).
22. Kong, L. *et al*. Electromagnetic wave absorption properties of reduced graphene oxide modified by maghemite colloidal nanoparticle clusters. *J. Phys. Chem. C* **117**, 19701–19711 (2013).
23. Wang, G. Z. *et al*. Microwave absorption properties of carbon nanocoils coated with highly controlled magnetic materials by atomic layer deposition. *ACS Nano* **6**, 11009–11017 (2012).
24. Zhang, D. F., Xu, F. X., Lin, J., Yang, Z. D. & Zhang, M. Electromagnetic characteristics and microwave absorption properties of carbon-encapsulated cobalt nanoparticles in 2-18-GHz frequency range. *Carbon* **80**, 103–111 (2014).
25. Fu, M., Jiao, Q. Z. & Zhao, Y. Preparation of $NiFe_2O_4$ nanorodgraphene composites via an ionic liquid assisted one-step hydrothermal approach and their microwave absorbing properties. *J. Mater. Chem. A* **1**, 5577–5586 (2013).
26. Zhao, H. B., Fu, Z. B., Chen, H. B., Zhong, M. L. & Wang, C. Y. Excellent electromagnetic absorption capability of Ni/carbon based conductive and magnetic foams synthesized via a green one pot route. *ACS Appl. Mater. Interface* **8**, 468–1477 (2016).
27. Wadhawan, A., Garrett, D. & Perez, J. M. Nanoparticle-assisted microwave absorption by single-wall carbon nanotubes. *Appl. Phys. Lett.* **83**, 2683–2865 (2003).
28. Kim, H. M. *et al*. Electrical conductivity and electromagnetic interference shielding of multiwalled carbon nanotube composites containing Fe catalyst. *Appl. Phys. Lett.* **84**, 589–591 (2004).
29. Zhang, X. F. *et al*. Microwave absorption properties of the carbon-coated nickel nanocapsules. *Appl. Phys. Lett.* **89**, 053115 (2006).
30. Qu, B., Zhu, C. L., Li, C. Y., Zhang, X. T. & Chen, Y. J. Coupling hollow Fe_3O_4-Fe nanoparticles with graphene sheets for high-performance electromagnetic wave absorbing material. *ACS Appl. Mater. Interface* **8**, 3730–3735 (2016).
31. Wang, Z. H., Choi, C. J., Kim, B. K., Kim, J. C. & Zhang, Z. D. Characterization and magnetic properties of carbon-coated cobalt nanocapsules synthesized by the chemical vapor-condensation process. *Carbon* **41**, 1751–1758 (2003).
32. Ang, K. H., Alexandrou, I., Mathur, N. D., Amaratunga, G. A. J. & Haq, S. The effect of carbon encapsulation on the magnetic properties of Ni nanoparticles produced by arc discharge in de-ionized water. *Nanotechnology* **15**, 520–524 (2004).
33. Park, J. B., Jeong, S. H., Jeong, M. S., Kim, J. Y. & Cho, B. K. Synthesis of carbonencapsulated magnetic nanoparticles by pulsed laser irradiation of solution. *Carbon* **46**, 1369–1377 (2008).
34. Sunny, V. *et al*. Synthesis and properties of highly stable nickel/carbon core/shell nanostructures. *Carbon* **48**, 1643–1651 (2010).
35. Liu, S. H. *et al*. Graphitically encapsulated cobalt nanocrystal assemblies. *Chem. Commun.* **46**, 4749–4751 (2010).

36. Zhao, Z. B., Qu, J. Y., Qiu, J. S., Wang, X. Z. & Wang., Z. Y. Water-assisted fabrication of aligned microsized carbon tubes made of self-assembled multi-wall carbon nanotubes. *Chem. Commun.* **6**, 594–596 (2006).
37. Hata, K. *et al*. Water-assisted highly efficient synthesis of impurity-free single-walled carbon nanotubes. *Science* **306**, 1362–1364 (2004).
38. Qi, X. S., Zhong, W., Deng, Y., Au, C. T. & Du, Y. W. Synthesis of helical carbon nanotubes, worm-like carbon nanotubes and nanocoils at 450 °C and their magnetic properties. *Carbon* **48**, 365–376 (2010).
39. Qi, X. S. *et al*. Large-scale synthesis, characterization and microwave absorption properties of carbon nanotubes of different helicities. *J. Solid State Chem.* **182**, 2691–2697 (2009).
40. Qi, X. S. *et al*. Simultaneous synthesis of carbon nanobelts and carbon/Fe–Cu hybrids for microwave absorption. *Carbon* **48**, 3512–3522 (2010).
41. Qi, X. S., Xu, J. L., Zhong, W. & Du, Y. W. A facile route to synthesize core/shell structured carbon/magnetic nanoparticles hybrid and their magnetic properties. *Mater. Res. Bull.* **67**, 162–169 (2015).
42. Jin, C. Q. *et al*. Synthesis and abnormal photoluminescence of core/shell structured Fe/ZnO nanoparticles. *J. Appl. Phys.* **103**, 07D520 (2008).
43. Tang, N. J. *et al*. Large-scale synthesis, annealing, purification, and magnetic properties of crystalline helical carbon nanotubes with symmetrical structures. *Adv. Funct. Mater.* **17**, 1542–1550 (2007).
44. Park, J. B., Jeong, S. H., Jeong, M. S., Kim, J. Y. & Cho, B. K. Synthesis of carbon-encapsulated magnetic nanoparticles by pulsed laser irradiation of solution. *Carbon* **46**, 1369–1377 (2008).
45. Wang, M. H. *et al*. Templated fabrication of core-shell magnetic mesoporous carbon microspheres in 3-dimensional ordered macroporous silicas. *Chem. Mater.* **26**, 3316–3321 (2014).
46. Zhang, H. M., Liang, C. H., Liu, J., Tian, Z. F. & Shao, G. S. The formation of onion-like carbon-encapsulated cobalt carbide core/shell nanoparticles by the laser ablation of metallic cobalt in acetone. *Carbon* **55**, 108–115 (2012).
47. Bystrzejewski, M. *et al*. Continuous synthesis of carbon-encapsulated magnetic nanoparticles with a minimum production of amorphous carbon. *Carbon* **47**, 2040–2048 (2009).
48. Tang, N. J. *et al*. Helical carbon nanotubes: catalytic particle size-dependent growth and magnetic properties. *ACS Nano* **4**, 241–250 (2010).
49. Qi, X. S., Xu, J. L., Hu, Q., Zhong, W. & Du, Y. W. Preparation, electromagnetic and enhanced microwave absorption properties of Fe nanoparticles encapsulated in carbon nanotubes. *Mater. Sci. Eng. B* **198**, 108–112 (2015).
50. Tang, N. J., Zhong, W., Gedanken, A. & Du, Y. W. High magnetization helical carbon nanofibers produced by nanoparticle catalysis. *J. Phys. Chem. B* **110**, 11772–11774 (2006).
51. Serp, P. *et al*. A chemical vapour deposition process for the production of carbon nanospheres. *Carbon* **39**, 621–626 (2001).
52. Lan, H. C. *et al*. Efficient conversion of dimethylarsinate into arsenic and its simultaneous adsorption removal over FeC_x/N-doped carbon fiber composite in an electro-Fenton process. *Water Res.* **100**, 57–64 (2016).
53. Yamashita, T. & Hayes, P. Analysis of XPS spectra of Fe^{2+} and Fe^{3+} ions in oxide materials. *Appl. Surf. Sci.* **254**, 2441–2449 (2008).
54. Li, J. X. *et al*. Fe-added Fe_3C carbon nanofibers as anode for Li ion batteries with excellent low-temperature performance. *Electrochim. Acta* **153**, 300–305 (2015).
55. Kishore, S. C., Anandhakumar, S. & Sasidharan, M. Direct synthesis of solid and hollow carbon nanospheres over NaCl crystals using acetylene by chemical vapour deposition. *Appl. Surf. Sci.* **400**, 90–96 (2017).
56. Zhao, N. Q. *et al*. Chemical vapor deposition synthesis of carbon nanospheres over Fe-based glassy alloy particles. *J. Alloys Compds.* **617**, 816–822 (2014).
57. He, C. *et al*. Direct synthesis of amorphous carbon nanotubes on $Fe_{76}Si_9B_{10}P_5$ glassy alloy particles. *J. Alloys Compds.* **581**, 282–288 (2013).
58. Zhao, Y., Choi, J., Kim, P., Fei, W. D. & Lee, C. J. Large-scale synthesis and characterization of super-bundle single-walled carbon nanotubes by water-assisted chemical vapor deposition. *RSC Adv.* **5**, 30564–30569 (2015).
59. Zhang, S. *et al*. From solid carbon sources to carbon nanotubes: a general water-assisted approach. *RSC Adv.* **4**, 54244–54248 (2014).
60. Yang, F. *et al*. Water-assisted preparation of high-purity semiconducting (14,4) carbon nanotubes. *ACS Nano* **11**, 186–193 (2017).
61. Liu, S. H., Zhang, Y. Y., Lin, Y., Zhao, Z. G. & Li, Q. W. Tailoring the structure and nitrogen content of nitrogen-doped carbon nanotubes by water-assisted growth. *Carbon* **69**, 247–254 (2014).
62. Zheng, Z., Xu, B., Huang, L., He, L. & Ni, X. M. Novel composite of Co/carbon nanotubes: synthesis, magnetism and microwave absorption properties. *Solid State Sci.* **10**, 316–320 (2008).
63. Liu, Z., Lv, C. & Tan, X. L. One-pot synthesis of Fe, Co and Ni-doped carbon xerogels and their magnetic properties. *J. Phys. Chem.* **74**, 1275–1280 (2013).
64. Wu, F., Xie, A. M., Sun, M. X., Wang, Y. & Wang, M. Y. Reduced graphene oxide (RGO) modified spongelike polypyrrole (PPy) aerogel for excellent electromagnetic absorption. *J. Mater. Chem. A* **3**, 14358–14369 (2015).
65. Kashi, S., Gupta, R. K., Baum, T., Kao, N. & Bhattacharya, S. N. Dielectric properties and electromagnetic interference shielding effectiveness of graphene-based biodegradable nanocomposites. *Mater. Des.* **109**, 68–78 (2016).
66. Khurram, A. A., Rakha, S. A., Zhou, P. H., Shafi, M. & Munir, A. Correlation of electrical conductivity, dielectric properties, microwave absorption, and matrix properties of composites filled with grapheme nanoplatelets and carbon nanotubes. *J. Appl. Phys.* **118**, 044105 (2015).
67. Chen, Y. *et al*. Fe_2O_3-MWNT/poly(p-phenylenebenzobisoxazole) composites with excellent microwave absorption performance and thermal stability. *Nanoscale* **6**, 6440–6447 (2014).
68. Qi, X. S. *et al*. Heteronanostructured Co@carbon nanotubes-graphene ternary hybrids: synthesis, electromagnetic and excellent microwave absorption properties. *Sci. Rep.* **6**, 37972 (2016).
69. Wang, L. N. *et al*. Synthesis and microwave absorption property of flexible magnetic film based on graphene oxide/carbon nanotubes and Fe_3O_4 nanoparticles. *J. Mater. Chem. A* **2**, 14940–14946 (2014).
70. Chen, D. Z. *et al*. Controllable fabrication of mono-dispersed RGO-hematite nanocomposites and their enhanced wave absorption properties. *J. Mater. Chem. A* **1**, 5996–6003 (2013).
71. Michielssen, E., Sager, J. M., Ranjithan, S. & Mittra, R. Design of lightweight, broad-band microwave absorbers using genetic algorithms. *Microwave Theory Tech.* **41**, 1024–1031 (1993).
72. Yusoff, A. N., Abdullah, M. H., Ahmad, S. H. & Jusoh, S. F. Electromagnetic and absorption properties of some microwave absorbers. *J. Appl. Phys.* **92**, 876–882 (2002).
73. Wen, F. S., Zhang, F. & Liu, Z. Y. Investigation on microwave absorption properties for multiwalled carbon nanotubes/Fe/Co/Ni nanopowders as lightweight absorbers. *J. Phys. Chem. C* **115**, 14025–14030 (2011).
74. Chen, Y. J. *et al*. Porous Fe_3O_4/carbon core/shell nanorods: synthesis and electromagnetic properties. *J. Phys. Chem. C* **115**, 13603–13608 (2011).
75. Zhu, C. L. *et al*. Fe_3O_4/TiO_2 core/shell nanotubes: synthesis and magnetic and electromagnetic wave absorption characteristics. *J. Phys. Chem. C* **114**, 16229–16235 (2010).
76. Wang, Z. J. *et al*. Magnetite nanocrystals on multiwalled carbon nanotubes as synergistic microwave absorber. *J. Phys, Chem. C* **117**, 5446–5452 (2013).
77. Qi, X. S. *et al*. Enhanced microwave absorption properties and mechanism of core/shell structured magnetic nanoparticles/carbon-based nanohybrids. *Mater, Sci. Eng. B* **211**, 53–60 (2016).

78. Zhao, X. C. *et al*. Excellent microwave absorption property of graphene-coated Fe nanocomposites. *Sci. Rep.* **3**, 3421 (2013).
79. Lv, H. L., Ji, G. B., Liang, X. H., Zhang, H. Q. & Du, Y. W. A novel rod-like MnO_2@Fe loading on grapheme giving excellent electromagnetic absorption properties. *J. Mater. Chem. C* **3**, 5056–5064 (2015).
80. Ren, Y. L. *et al*. Quaternary nanocomposites consisting of graphene, Fe_3O_4@Fe core@shell, and ZnO nanoparticles: synthesis and excellent electromagnetic absorption properties. *ACS Appl. Mater. Interface* 4, (6436–6442 (2012).
81. Lv, H. L. *et al*. Co_xFe_y@C composites with tunable atomic ratios for excellent electromagnetic absorption properties. *Sci. Rep.* **5**, 18249 (2015).
82. Ren, Y. L., Zhu, C. L., Qi, L. H., Gao, H. & Chen, Y. J. Growth of γ-Fe_2O_3 nanosheet arrays on graphene for electromagnetic absorption applications. *RSC Adv.* **4**, 21510–21516 (2014).
83. Zhang, H. M., Zhu, C. L., Chen, Y. J. & Gao, H. Growth of Fe_3O_4 nanorod arrays on graphene sheets for application in electromagnetic absorption fields. *ChemPhysChem* **15**, 2261–2266 (2014).
84. Liu, P. B., Huang, Y., Yan, J. & Zhao, Y. Magnetic graphene@PANI@porous TiO_2 ternary composites for high-performance electromagnetic wave absorption. *J. Mater. Chem. C* **4**, 6362–6370 (2016).
85. Wu, T. *et al*. Facile hydrothermal synthesis of Fe_3O_4/C core-shell nanorings for efficient low-frequency microwave absorption. *ACS Appl. Mater. Interfaces* **8**, 7370–7380 (2016).

Acknowledgements

This work was supported by the Graduate Innovation Fund of Guizhou University (2016–015), the Innovation and Entrepreneurship Training Program for University Student (2016–004), the Excellent Talents of Guizhou Province (2014–239), the National Science Foundation of Guizhou province (2014–2059), the Postdoctoral Science Foundation of China (2015M570427), the Science and Technology Innovation Team of Guizhou province (2015–4017), the National Science Foundation of China (Grant Nos. 11364005, 11474151 and 11604060), and the Foundation of the National Key Project for Basic Research (2012CB932304) for financial support.

Author Contributions

E.Q. Yang, H.B. Cai and X.S. Qi are the joint first author, they contributed equally to this work. R. Xie, Z.C. Bai and Y. Jiang collected the experimental data. Results were analyzed and interpreted by X.S. Qi, S.J. Qin, W. Zhong and Y.W. Du. The manuscript was written by X.S. Qi and W. Zhong.

Additional Information

Supplementary information accompanies this paper at doi:10.1038/s41598-017-10352-8

Competing Interests: The authors declare that they have no competing interests.

Publisher's note: Springer Nature remains neutral with regard to jurisdictional claims in published maps and institutional affiliations.